



Modelling the Role of Cell–Cell Adhesion in the Growth and Development of Carcinomas

H. M. BYRNE[†] AND M. A. J. CHAPLAIN

School of Mathematical Sciences, University of Bath

Claverton Down, Bath BA2 7AY, U.K.

<hmb><majc>@maths.bath.ac.uk

(Received March 1996; revised and accepted July 1996)

Abstract—In this paper, a mathematical model is presented to describe the evolution of an avascular solid tumour in response to an externally-supplied nutrient. The growth of the tumour depends on the balance between expansive forces caused by cell proliferation and cell–cell adhesion forces which exist to maintain the tumour’s compactness. Cell–cell adhesion is incorporated into the model using the Gibbs–Thomson relation which relates the change in nutrient concentration across the tumour boundary to the local curvature, this energy being used to preserve the cell–cell adhesion forces.

Our analysis focuses on the existence and uniqueness of steady, radially-symmetric solutions to the model, and also their stability to time-dependent and asymmetric perturbations. In particular, our analysis suggests that if the energy needed to preserve the bonds of adhesion is large then the radially-symmetric configuration is stable with respect to all asymmetric perturbations, and the tumour maintains a radially-symmetric structure—this corresponds to the growth of a benign tumour. As the energy needed to maintain the tumour’s compactness diminishes so the number of modes to which the underlying radially-symmetric solution is unstable increases—this corresponds to the invasive growth of a carcinoma. The strength of the cell–cell bonds of adhesion may at some stage provide clinicians with a useful index of the invasive potential of a tumour.

Keywords—Cell adhesion, Cancer, Asymmetric tumour growth.

1. INTRODUCTION

One of the reasons why successful treatment of cancer remains such a challenging problem is the diversity in behaviour exhibited by different tumours. Thus, whilst a putative anticancer drug may perform well on multicellular spheroids in the laboratory, the same drug may fail to elicit the same response *in vivo*. This discrepancy could be attributed to discernible differences in tumour structure. For example, well-developed multicellular spheroids tend to possess a common structure, which comprises a central core of nutrient-starved, necrotic cells, surrounded by proliferating cells restricted to the nutrient-rich outer layer of the tumour [1–3]. A quiescent population may also exist “sandwiched” between the two. *In vivo* cancer growth is, by contrast, less reproducible and less well defined, with heterogeneity occurring over much shorter length-scales (\sim several cells *in vivo*, as opposed to \sim millimetres *in vitro*), so that necrotic cells may be adjacent to both proliferating and quiescent cells [4]. A further difference between *in vitro* and *in vivo* tumour growth arises from the ability of tumours grown *in vivo* to induce blood vessels from the surrounding tissue to form a capillary network which migrates towards, and ultimately penetrates, the tumour, thereby providing it with an adequate blood supply and microcirculation.

[†]Present address: Department of Applied Mathematics, UMIST, P.O. Box 88, Manchester M60 1QD, U.K.

This process is called angiogenesis [5-8] and marks the transition from the relatively harmless, and localised, avascular state described above to the more dangerous, vascular state, wherein the tumour possesses the ability to invade surrounding tissue and metastasise to distant parts of the body. The rapid increase in cell proliferation that occurs during vascular growth can cause large interstitial pressures to be created at the centre of the tumour. These may be sufficient to occlude blood vessels at the centre of the tumour, thereby restricting the delivery of anticancer drugs to the tumour [9,10], and providing some explanation for why some *in vivo* tumours respond less favourably to a course of treatment than anticipated. A further feature of malignant tumours (cancers) is their propensity for invasion. Thus, whilst multicellular spheroids maintain an approximately spherical structure as they grow, cancers (e.g., carcinoma) may develop finger-like protrusions of invading cells and evolve with a less well-defined, or asymmetric, outer boundary. In this paper, we develop a mathematical model which, we believe, provides some insight into the *physical effects* which may be responsible for the differing degrees of invasion exhibited by different types of tumours.

Progress in modelling tumour growth has been largely guided by experimental results. Thus, many of the mathematical models in the literature focus on the growth of (avascular) multicellular spheroids. These models generally consist of an ordinary differential equation (ODE), coupled to one or more reaction-diffusion equations (RDEs) [11-18]. The ODE derives from mass conservation applied to the tumour and describes the evolution of the tumour boundary, whereas the RDEs describe the distribution, within the tissue, of vital nutrients, such as oxygen and glucose, and growth inhibitory factors. In these models no explicit mention of the constituent tumour cells is made. Instead, it is assumed that the nutrient level at each point within the tumour provides an index of the cell type there. Thus, high nutrient levels indicate cell mitosis, moderate levels indicate quiescence, and low levels necrosis. Such models accurately reproduce not only the growth of spheroids but also the macroscopic heterogeneity described above. As such, they show good qualitative agreement with experimental results. The models also indicate how the relative magnitude of the system parameters which describe the tumour's handling of vital nutrients and growth inhibitors affect the limiting structure of the spheroid. Mathematical models also exist which show *quantitative* consistency with spheroid growth data, for example, [19,20].

Several models have been proposed to describe the process of angiogenesis described above [21-25]. In these models the success with which a tumour can establish its own vascular supply is shown to depend on system parameters such as the distance to the nearest vascular bed, the rate at which new tips proliferate, and the speed with which they migrate towards the tumour.

As mentioned above, the ability with which they invade their host environment is a further means of classifying tumours. Thus, whilst multicellular spheroids maintain their compact spherical form as they grow, carcinomas *in vivo* typically present a less well-defined, or asymmetric, outer boundary [26]. In this paper, we develop a mathematical model which enables us to assess how changes in the relative importance of competing physical effects affect a tumour's potential for invasion. In particular, we suggest that it is the balance between an internal expansive force and a restraining force which determines whether the tumour grows or regresses, and whether its outer boundary remains radially symmetric when subject to small asymmetric perturbations. The internal force is caused by cell proliferation within the tumour, whereas the restraining force is due to intercellular bonds of adhesion which exist between cells in the periphery of the tumour and which serve to maintain the colony's compactness [26].

The derivation of the original model is similar to that developed by Greenspan to describe the growth of a tumour in response to an externally-supplied nutrient [27]. Like Greenspan, we assume that the tumour acts as an incompressible fluid, and hence, that local changes in the cell population, caused by the birth or death of cells, will give rise to internal pressure gradients which act as expansive forces, inducing cell motion and producing the expansion of the tumour colony. Unlike Greenspan, who assumes that the tumour comprises a large necrotic core, enveloped by a thin rim of proliferating cells, we shall assume that the tumour consists of

proliferating cells only—it does not contain a central necrotic core. (This assumption can easily be relaxed and is adopted here simply for clarity of exposition.) Perhaps the most significant difference between Greenspan's and our model is the manner in which so-called surface tension effects are incorporated. Greenspan assumes that, on the surface of the tumour, the surface tension force, which exists to maintain compactness, balances the internal expansive pressure per unit surface area. Working on an infinite domain, he assumes further that the nutrient concentration is continuous across the tumour boundary, but that the flux of nutrient is not. By contrast we restrict attention to the moving domain defined by the tumour volume and incorporate surface tension effects by assuming that the nutrient concentration satisfies the Gibbs-Thomson relation on the boundary [28,29]. The Gibbs-Thomson relation states that the nutrient concentration at a point on the tumour boundary is less than the (assumed constant) external concentration by a factor which depends on the local curvature there. This energy is needed by cells on the periphery in order to preserve the forces of adhesion which exist to maintain the tumour's compactness. Previous models examining the morphogenetic changes in cell and subcellular structure include [30–35], while clear experimental evidence for these effects can be found in [36,37] and references therein.

In vitro observations [1,4,38], suggest that in the early stages solid tumours remain approximately spherically symmetric as they grow. Therefore, our analysis focuses on the existence, and stability, of radially-symmetric solutions of the model equations. As a consequence of seeking radially-symmetric solutions, we show how the pressure variable can be eliminated from the model and how a (reduced) system of equations, which is similar in form to the models of multicellular spheroids proposed by Adam, Greenspan, and others [11–15,17,18,39], can be recovered. We believe that our derivation of this simplified model indicates how models of avascular tumour growth, such as those proposed by Adam and others, arise as special cases of more physically-based models.

Solution of the radially-symmetric model shows how the existence and stability, with respect to time-dependent perturbations, depends on the system parameters. For example, referring to Figures 2 and 3, we deduce that if the bonds of cell-cell adhesion are strong enough, relative to the other physical effects, then no steady state solutions exist and no tumour will persist in the tissue. By contrast, if the bonds of adhesion are weak enough then two steady states are predicted, of which the smaller is unstable with respect to temporal perturbations, whereas the larger tumour is not.

Our analysis of the reduced model also investigates how small deviations from radial symmetry develop in time and focuses, in particular, on the role played by cell-cell adhesion in the developing structure. If all asymmetric perturbations ultimately disappear, then we conclude that the tumour will grow as a radially-symmetric mass with no invasion. By contrast, the growth of a perturbation implies that the tumour has a propensity for asymmetric invasion, the growth rate of the perturbation indicating the degree of aggression.

2. MODEL FORMULATION

We consider an avascular solid tumour which consists of proliferating cells only and whose growth is regulated by an externally supplied nutrient, such as oxygen or glucose.

Denoting by $c(r, t)$, the nutrient concentration at a point inside the tumour, we assume that the evolution of c can be described by a reaction-diffusion equation (RDE). Now, of the two timescales associated with tumour growth, the nutrient diffusion timescale (\sim minutes) is much shorter than the tumour doubling time, or growth timescale (\sim days) [14]. Thus, as the tumour grows, the nutrient rapidly redistributes itself throughout the new volume. Following [11,17,39], we scale time with the tumour growth timescale and set $\frac{\partial}{\partial t} \equiv 0$ in the nutrient RDE. Assuming further that the diffusion coefficient is constant ($= 1$, by suitable rescaling) and that nutrient is consumed by proliferating cells at the rate $\lambda(c)$, we propose the following quasisteady RDE to

describe the distribution of c within the tumour:

$$0 = \nabla^2 c - \lambda(c). \quad (2.1)$$

If we regard the tumour as an incompressible fluid, then local changes in the cell population, caused by, say, the birth and death of cells, will induce motion of neighbouring cells. Assuming further that the net proliferation rate S at a point inside the tumour can be expressed in terms of the nutrient concentration there, we set $S = S(c)$. Introducing the cell velocity $\mathbf{u}(r, t)$ and applying mass conservation, we derive the following equation for \mathbf{u} :

$$\nabla \cdot \mathbf{u} = S(c). \quad (2.2)$$

Denoting the outer surface of the tumour colony by the free boundary $\Gamma(r, t) = 0$, where

$$\Gamma(r, t) = 0 = r - R(\theta, \phi, t),$$

the equation of motion of a point on $\Gamma(r, t) = 0$ is given by

$$\hat{\mathbf{n}} \cdot \frac{d\mathbf{r}}{dt} = \mathbf{u} \cdot \hat{\mathbf{n}}, \quad (2.3)$$

where $\hat{\mathbf{n}}$ is an outward unit normal. Subject to boundary and initial conditions described below, equations (2.1)–(2.3) define the evolution of the nutrient concentration, the cell velocity and the outer tumour boundary. In the following analysis, it is convenient to reformulate the above problem in terms of a related dependent variable, the internal pressure p . (In particular, this modification will facilitate comparisons with Greenspan's model [27].) We assume that \mathbf{u} is related to p via Darcy's Law [40]

$$\mathbf{u} = -\mu \nabla p,$$

where μ denotes the motility of the tumour cells. (We remark that Darcy's Law is often used to describe the flow of a fluid or gas through a porous medium [41]. Given its heterogeneous structure, it seems reasonable that the internal microstructure of the tumour can be described as a porous medium and that Darcy's Law can be used to model the motion of the tumour cells through the tumour matrix.) Thus, changes in the local density lead to variations in p , which in turn, induce motion of the constituent tumour cells. Eliminating \mathbf{u} in favour of the scalar field p , equations (2.2) and (2.3) transform to give

$$\mu \nabla^2 p = -S(c), \quad (2.4)$$

$$\hat{\mathbf{n}} \cdot \frac{d\mathbf{r}}{dt} = -\mu \nabla p \cdot \hat{\mathbf{n}}, \quad \text{on } \Gamma(r, t) = 0. \quad (2.5)$$

Referring to (2.1), for bounded solutions we impose $\frac{\partial c}{\partial r} = 0$ at $r = 0$. In addition, the nutrient concentration on the tumour boundary is prescribed. Denoting by c_∞ , the constant nutrient concentration in the external tissue, we note that, to date, most authors assume that the nutrient concentration is continuous across $\Gamma(r, t) = 0$ so that $c = c_\infty$ there [11–18]. Here this assumption is relaxed. By assuming that adhesive forces exist between cells on the tumour boundary, in order to maintain the tumour's structure, we postulate that it is the balance between these stabilising, or restraining, forces and the expansive force caused by internal cell proliferation which determines whether the tumour colony expands or regresses in time. Now, we assume that energy is expended in maintaining the peripheral cell–cell bonds, the requisite amount of energy increasing with the local curvature of the boundary. Assuming that the nutrient acts as a source of this energy, we assume that c satisfies the Gibbs-Thomson relation on $\Gamma(r, t) = 0$ (see (2.7)). This relation states that the nutrient concentration on the tumour boundary is less than the external concentration by a factor which depends on the curvature there [28,29]. In other words,

denoting by κ the mean curvature and by 2γ , the surface tension per unit surface area, the amount of energy needed to maintain the tumour's structure at a given point on $\Gamma(r, t) = 0$ is given by $2c_\infty\gamma\kappa$.

Turning now to the internal pressure field p for bounded solutions, we impose $\frac{\partial p}{\partial r} = 0$ at $r = 0$. In addition, we assume that on the tumour boundary p matches continuously with the external pressure field where $p = p_\infty$. Thus, we impose $p = p_\infty$ on $\Gamma(r, t) = 0$. Finally, we prescribe the initial tumour boundary $\Gamma(r, 0) = 0$. In summary, the following boundary and initial conditions are applied to equations (2.1), (2.4), and (2.5):

$$\frac{\partial c}{\partial r} = 0, \quad \text{at } r = 0, \quad (2.6)$$

$$c = c_\infty(1 - 2\gamma\kappa), \quad \text{on } \Gamma(r, t) = 0, \quad (2.7)$$

$$\frac{\partial p}{\partial r} = 0, \quad \text{at } r = 0, \quad (2.8)$$

$$p = p_\infty, \quad \text{on } \Gamma(r, t) = 0, \quad (2.9)$$

$$\Gamma(r, 0) = 0 = r - R(\theta, \phi, 0), \quad \text{prescribed.} \quad (2.10)$$

Model Simplification—Radial Symmetry

Under conditions of spherical symmetry, the dependent variables depend only on r and t , and the tumour grows as a sphere of radius $R(t)$, with curvature $\kappa = 1/R$. In this case, the boundary value problem summarised in equations (2.1), (2.4)–(2.10) simplifies to give

$$0 = \frac{1}{r^2} \frac{\partial}{\partial r} \left(r^2 \frac{\partial c}{\partial r} \right) - \lambda(c), \quad (2.11)$$

$$0 = \frac{\mu}{r^2} \frac{\partial}{\partial r} \left(r^2 \frac{\partial p}{\partial r} \right) + S(c), \quad (2.12)$$

$$\frac{dR}{dt} = -\mu \frac{\partial p}{\partial r} \Big|_{r=R(t)}, \quad (2.13)$$

subject to

$$\frac{\partial c}{\partial r} = 0, \quad \text{at } r = 0, \quad (2.14)$$

$$c = c_\infty \left(1 - \frac{2\gamma}{R} \right), \quad \text{on } r = R, \quad (2.15)$$

$$\frac{\partial p}{\partial r} = 0, \quad \text{at } r = 0, \quad (2.16)$$

$$p = p_\infty, \quad \text{on } r = R, \quad (2.17)$$

$$R(0) = R_0, \quad \text{prescribed.} \quad (2.18)$$

We remark that in equations (2.11)–(2.13) the lowest order derivative of the pressure field is $\frac{\partial p}{\partial r}$. Further, integrating (2.12) from $r = 0$ to $r = R(t)$ yields the following expression which relates the pressure gradient on the boundary of the tumour to the rate of cell proliferation throughout the tumour volume:

$$\mu R^2 \frac{\partial p}{\partial r} \Big|_{r=R} = \mu \int_0^R \frac{\partial}{\partial r} \left(r^2 \frac{\partial p}{\partial r} \right) dr = - \int_0^R S(c) r^2 dr.$$

Substituting with this identity in (2.13), the pressure field p can be eliminated from the governing equations and our model for radially-symmetric tumour growth reduces to give

$$0 = \frac{1}{r^2} \frac{\partial}{\partial r} \left(r^2 \frac{\partial c}{\partial r} \right) - \lambda(c), \quad (2.19)$$

$$R^2 \frac{dR}{dt} = \int_0^R S(c) r^2 dr, \quad (2.20)$$

subject to

$$\frac{\partial c}{\partial r} = 0, \quad \text{at } r = 0, \quad (2.21)$$

$$c = c_\infty \left(1 - \frac{2\gamma}{R}\right), \quad \text{on } r = R, \quad (2.22)$$

$$R(0) = R_0, \quad \text{prescribed.} \quad (2.23)$$

We remark further that (2.20) can be rewritten as follows:

$$\frac{d}{dt} \left(\frac{\text{tumour}}{\text{volume}} \right) = \frac{d}{dt} \left(\frac{4}{3} \pi R^3 \right) = \iiint_{\text{tumour}} S(c) dV.$$

Thus, (2.20) states that the rate of increase of the tumour volume is equal to the net tumour cell proliferation rate, taken over the entire tumour. Many authors have proposed models of this form (with $\gamma = 0$ in (2.22)) to describe avascular tumour growth, without referring to either the internal pressure field or the cell velocity. We believe that our derivation of equations (2.19)–(2.23) shows how such models of avascular tumour growth can arise as special cases of more physically-based models, such as the original model presented in Section 2.

Once the interaction terms $\lambda(c)$ and $S(c)$ have been specified, it is possible to determine the evolution of the tumour colony. In Section 3, we derive explicit solutions for $c(r, t)$ and $R(t)$ for simple choices of λ and S .

As natural extensions of the model proposed here, it is possible to investigate the action of different anticancer drugs on the tumour's growth and also the impact of the host's immune response [14,15]. These generalisations may be effected by incorporating into the model a second, inhibitory chemical species, β say, which describes the concentration of the anticancer drug, or the inhibitory chemical secreted by the host tissue in response to the foreign body [14,15]. Like the nutrient σ , the inhibitor β satisfies a quasisteady reaction-diffusion equation. The efficacy of different inhibitory mechanisms can be tested by considering different choices of the nutrient consumption rate ($\gamma \rightarrow \gamma_\sigma(\sigma, \beta)$), the inhibitor consumption rate ($\gamma_\beta = \gamma_\beta(\sigma, \beta)$), and the cell proliferation rate ($S = S(\sigma, \beta)$).

3. RADially-SYMMETRIC TUMOUR GROWTH

We now construct explicit solutions for $c(r, t)$ and $R(t)$ for particular choices of the interaction terms $\lambda(c)$ and $S(c)$. Whilst experimentally-determined functional forms for λ and S should be employed, they are not considered here since they are not amenable to simple mathematical analysis. Instead, merely as an illustrative example, we consider simple choices for λ and S , the results presented below indicating that even these expressions give rise to qualitatively realistic tumour behaviour.

Specifically, we assume that nutrient is consumed by proliferating cells at a constant rate so that, in equation (2.19),

$$\lambda(c) = \lambda, \quad \text{constant.}$$

The local proliferation rate is governed by the balance between cell mitosis and natural cell death or apoptosis [2,3]. Assuming that cells divide at the rate sc and die at the constant rate $s\bar{c}$, we obtain the following expression for $S(c)$ inside the tumour:

$$S(c) = s(c - \bar{c}).$$

With $\lambda(c) = \lambda$, so that the rate of nutrient consumption by the tumour cells is constant, integrating (2.19) subject to (2.21) and (2.22), we obtain the following expression for $c(r, t)$ in terms of the moving boundary $R(t)$:

$$c(r, t) = c_\infty \left(1 - \frac{2\gamma}{R}\right) - \frac{\lambda}{6} (R^2 - r^2). \quad (3.1)$$

From (3.1), we note that c increases monotonically from $r = 0$ to $r = R$. This agrees qualitatively with experimental results [42]. Now if the nutrient concentration falls below a critical value, c_{nec} say, then the tumour cells, being deprived of vital nutrients, undergo necrosis and die [2-4, 38,42]. In this paper, we restrict attention to nonnecrotic configurations. Since c attains its minimum value at $r = 0$, we deduce that for valid (nonnecrotic) solutions the following inequality must be satisfied:

$$c(0, t) = c_\infty \left(1 - \frac{2\gamma}{R} \right) - \frac{\lambda R^2}{6} > c_{nec}. \tag{3.2}$$

For fixed parameter values this relation restricts the range of R for which nonnecrotic solutions exists. When $\gamma = 0$, (3.2) simply provides an upper bound on the radius of nonnecrotic tumours. For larger radii, tumour necrosis is predicted. The inclusion of cell-cell adhesion into the model ($\gamma > 0$) introduces a nonzero lower bound for R . Following [28,29], we interpret this as a nucleation radius: for smaller tumour radii the continuum approach adopted here ceases to apply.

Before continuing, we remark that, with $c(r, t)$ defined by (3.1), the internal pressure field can now be determined by integrating (2.12) and imposing (2.16),(2.17). This yields the following expression for $p(r, t)$:

$$p(r, t) = p_\infty + \frac{s\lambda}{120\mu} (R^4 - r^4) + \frac{s}{6\mu} \left(c_\infty - \tilde{c} - \frac{2\gamma c_\infty}{R} - \frac{\lambda R^2}{6} \right) (R^2 - r^2).$$

Thus, we notice that inside the tumour the pressure increases as r decreases, attaining its *maximum value at the centre*. This agrees qualitatively with experimental results reported by Jain *et al.* [10] but is in contrast with the profile derived in Greenspan's model [27].

Substituting with $c(r, t)$ in (2.20) reduces the model to a nonlinear ODE for $R(t)$

$$\frac{1}{s} \frac{dR}{dt} = -\frac{2\gamma c_\infty}{3} + (c_\infty - \tilde{c}) \frac{R}{3} - \frac{\lambda R^3}{45}, \quad \text{with } R(t=0) = R_0. \tag{3.3}$$

The term $-2\gamma c_\infty/3$ in equation (3.3) renders explicit the stabilising effect that cell-cell adhesion has on the tumour's growth rate. The terms $-\tilde{c}R/3$ and $-\lambda R^3/45$ also show how nutrient consumption by the tumour cells and cell loss due to apoptosis together with cell-cell adhesion balance the destabilising expansive force due to cell proliferation, $c_\infty R/3$. Equations (3.3) provides us with some insight into the relative importance of these different mechanisms at different stages of the tumour's development. For example, assuming that all the parameters are $O(1)$, we deduce from (3.3) that when $0 < R \ll 1$, then cell-cell adhesion dominates the tumour's growth, whereas if $R \gg 1$, then nutrient consumption dominates.

Sketches of (3.3) in the $(R, \frac{dR}{dt})$ -plane show that the system possesses at most two, feasible steady solutions for which $\frac{dR}{dt} = 0$ and $R = R_\infty \geq 0$, the exact number of solutions depending on the system parameters. This situation is illustrated in Figure 1 where (3.3) is sketched for several choices of c_∞ , holding $\gamma, \lambda, \tilde{c}, c_{nec}$, and s fixed, with the growth rate calculated only for the permissible range of R , as defined by (3.2). The diagram provides some indication of the stability, with respect to time-dependent perturbations, of the steady state solutions, the arrows on each curve indicating the direction of growth of the tumour for a particular value of R , open circles denoting unstable steady states and closed circles denoting stable steady states [14]. When $c_\infty = 1.0$, no steady solutions occur and $\frac{dR}{dt} < 0$ for all values of R . Thus, for any feasible initial value of $R(t=0) = R_0$, the tumour radius decreases monotonically until it becomes so small that (3.2) is violated and the continuum model ceases to apply. When $c_\infty = 1.2$, two steady solutions are predicted: a small, unstable solution and a larger, stable solution. In this case, the limiting behaviour of the tumour depends on its starting value R_0 : if R_0 is smaller than the unstable steady state, then the tumour decays monotonically until it reaches the nucleation radius and the continuum model breaks down; if R_0 lies between the two steady state solutions, then the tumour

(3.1)

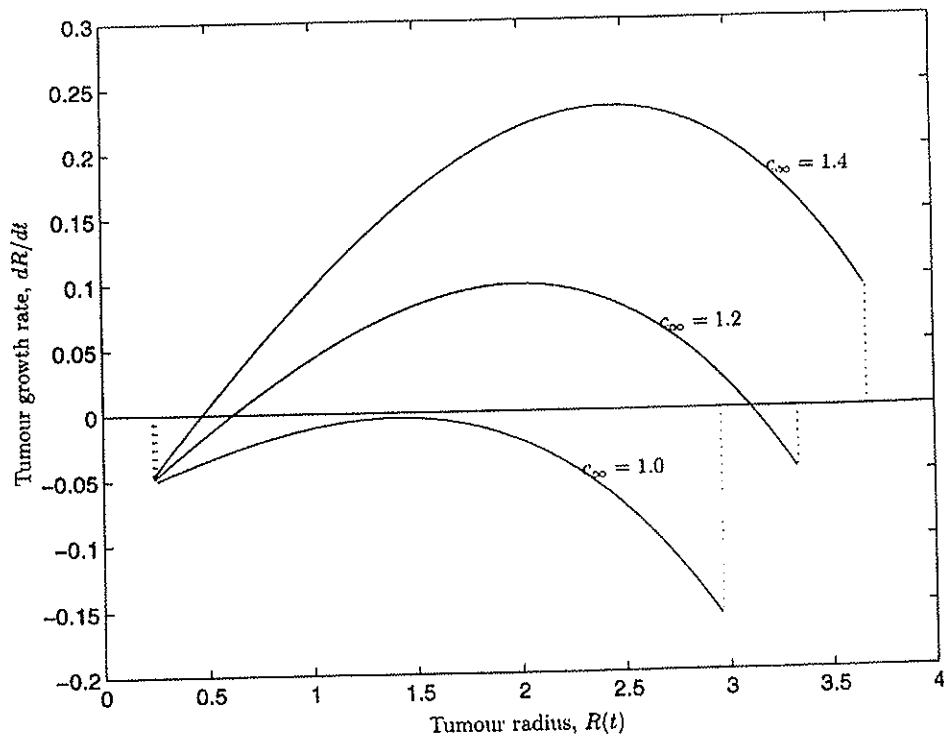


Figure 1. Diagram showing how a tumour's growth rate ($\frac{dR}{dt}$) varies with its radius (R) for three choices of c_∞ , and with $\frac{dR}{dt}$ calculated only within the feasible range of R as defined by (3.2). The arrows on each curve indicate the direction of growth of the tumour for a given value of R . Open circles denote unstable steady state solutions, whereas closed circles denote stable steady states. When $c_\infty = 1.0$, no steady solutions occur and $\frac{dR}{dt} < 0, \forall R$. When $c_\infty = 1.2$, one unstable solution and one (larger) stable solution are observed. When $c_\infty = 1.4$, only the unstable steady solution is observed—the larger solution is rejected since it develops a necrotic core. Parameter values: $\bar{c} = 0.8, c_{nec} = 0.2, \lambda = 0.5, \gamma = 0.1, s = 1.0$.

expands monotonically to the larger, stable steady state configuration; finally, if R_0 exceeds the larger steady state radius, then the tumour decreases monotonically to this stable value. (It will be interesting to compare these preliminary observations with the analysis of Section 4 where stability of the tumour with respect to asymmetric perturbations is considered.) As c_∞ increases, the larger steady solution grows and the nutrient concentration at the centre of the tumour falls until, eventually, necrosis is predicted and the larger solution leaves the range of validity. Thus, when $c_\infty = 1.4$, only one, unstable nonnecrotic solution is realised. By extending the model to include more developed tumour structures, it should be possible to demonstrate the existence of a tumour with a necrotic core for such parameter values [15]. When $c_\infty = 1.4$, the evolution of the tumour depends crucially on its value, the details of its behaviour mirroring that described above for the case $c_\infty = 1.2$.

Neglecting cell-cell adhesion, so that $\gamma = 0$, we note that the trivial, tumour-free state $R = 0$ satisfies (3.3). If, in addition, $c_{nec} < c_\infty < \bar{c}$, then the trivial solution is both unique and stable with respect to time-dependent perturbations [14]. More generally, introducing the parameter groupings

$$p_0 = \frac{30\gamma c_\infty}{\lambda} \quad \text{and} \quad p_1 = \frac{15}{\lambda} (c_\infty - \bar{c}), \quad (3.4)$$

and setting $\frac{dR}{dt} = 0$ in (3.3), we obtain the following cubic equation, whose roots correspond to the steady solutions of (3.3):

$$0 = R^3 - p_1 R + p_0. \quad (3.5)$$

Simple analysis shows that the existence and multiplicity of positive solutions of (3.5) can be related to the parameters p_0 and p_1 as follows:

$$\left(\frac{p_0}{2}\right)^2 - \left(\frac{p_1}{3}\right)^3 \begin{cases} > 0 & \Rightarrow \text{no real, positive solutions;} \\ = 0 & \Rightarrow \text{one, repeated solution;} \\ < 0 & \Rightarrow \text{two positive solutions.} \end{cases}$$

This situation is depicted in Figure 2 where (p_0, p_1) parameter space is partitioned into regions in which zero, one, or two nonnegative solutions exist. In Figure 3, we show how the radii of the corresponding tumours vary with p_0 as the trajectory shown in Figure 2 is described. Holding p_1 fixed, we observe that as p_0 increases from zero, the larger tumour radius decreases in size and the smaller one increases until $(p_0/2)^2 = (p_1/3)^3$ when the two tumours are the same size. For larger values of p_0 , no steady state solutions exist. The dashed curve, also included in Figure 3, shows how the range of R for which time-dependent, nonnecrotic solutions exist varies with p_0 . Outside this range, inequality (3.2) is violated and necrosis is predicted.

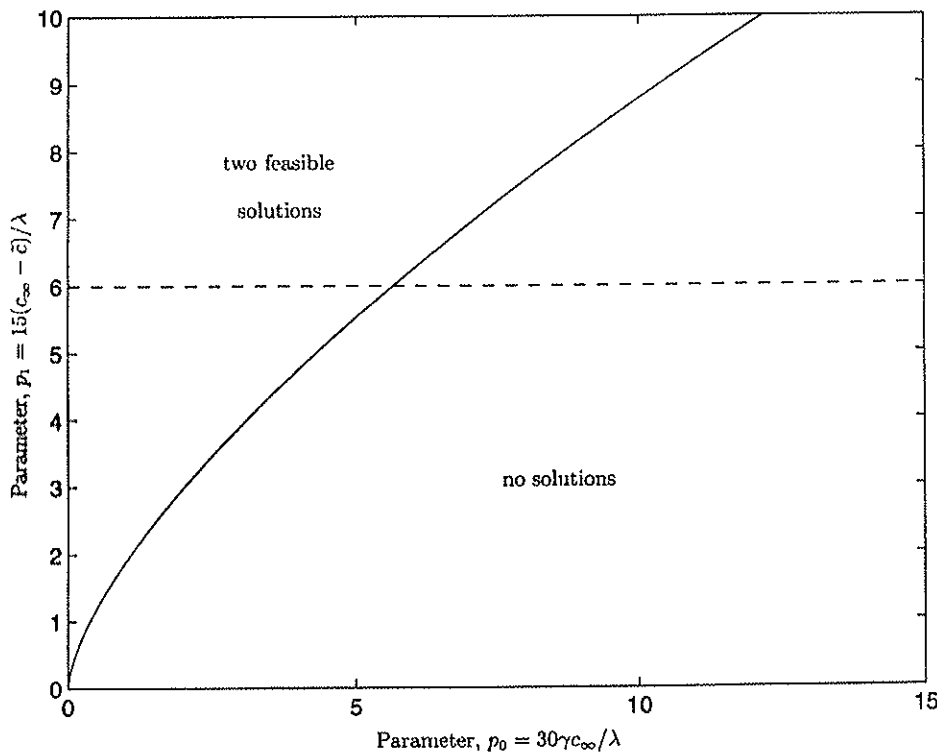


Figure 2. Diagram showing the domain of existence of nonnegative, radially-symmetric steady solutions with respect to the parameter groupings $p_0 = 30\gamma c_\infty/\lambda$ and $p_1 = 15(c_\infty - \delta)/\lambda$. The region in which two steady state solutions exist is separated from a region in which no steady solutions exist by the curve $(p_0/2)^2 = (p_1/3)^3$ along which one, degenerate steady solution exists.

From the definitions of p_0 and p_1 , we remark that holding p_1 fixed and increasing p_0 is equivalent to increasing the strength of the cell-cell bonds of adhesion γ , holding all other parameters fixed. Thus, we deduce from Figure 3 that if the bonds of adhesion between tumour cells are strong, then the tumour is likely to disappear. However if the bonds between the cells are weak, then the tumour will persist and eventually develop into a highly structured entity, with distinct regions of necrosis and quiescence. By measuring γ for different cell-lines, it should be possible to validate the predicted correlation between the strength of the cell-cell bonds of adhesion and the limiting size of the (avascular) tumour when grown *in vitro*. It might ultimately prove informative to use γ as a physical index which characterises a particular cell-line's potential for growth and invasion.

eds the
(It will
where
creases,
our falls
. Thus,
odel to
ence of
ition of
scribed

$R = 0$
l stable
parameter

(3.4)

pond to

(3.5)

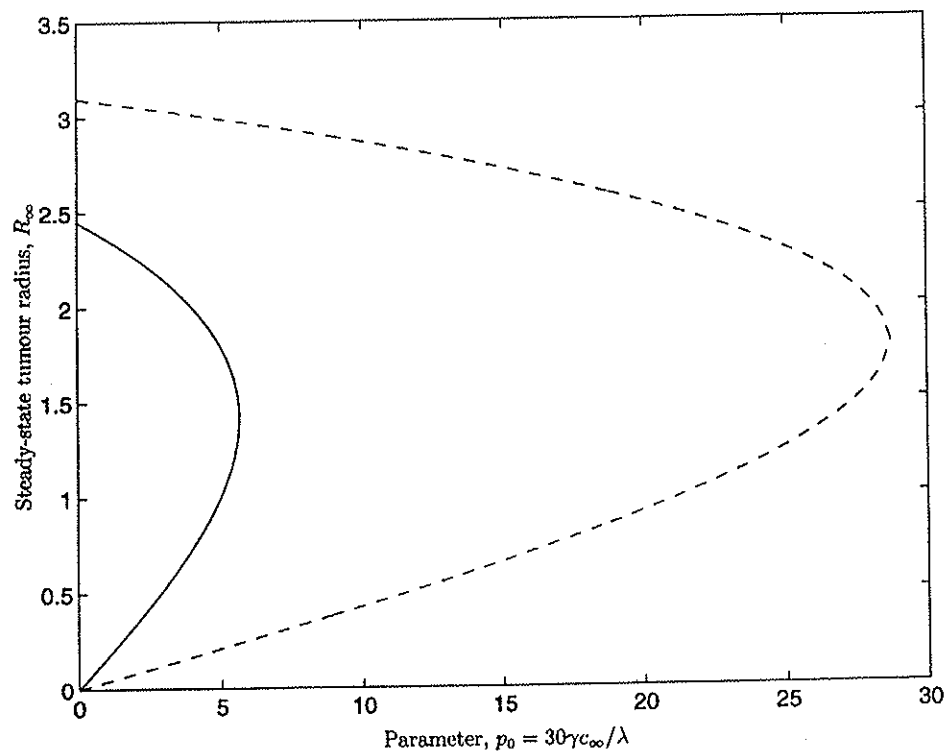


Figure 3. Diagram showing how the existence, uniqueness and magnitude of the steady state tumour radii depend on the parameter $p_0 = 30\gamma c_\infty/\lambda$. Fixing $p_1 = 15(c_\infty - \bar{c})/\lambda = 6.0$, the dashed curve shown in Figure 2 is described. For small values of p_0 ($0 \leq p_0 < 4$) two nontrivial steady solutions are predicted: for larger values of p_0 , no steady solutions occur. The dashed curve also included defines, for each value of p_0 (or γ), the range of R for which (time-dependent) nonnecrotic solutions exist (see equation (3.2)). Parameter values: $c_\infty = 1.0$, $\bar{c} = 0.8$, $c_{nec} = 0.2$, $\lambda = 0.5$, $s = 1.0$.

4. ASYMMETRIC GROWTH

We now derive equations which describe how small perturbations from radial symmetry evolve in time. For those cases in which instability of the asymmetric perturbations is predicted the shape of the tumour may alter radically from the spherically symmetric configuration, giving rise to configurations which are reminiscent of invasive carcinomas.

Introducing the small parameter $0 < \epsilon \ll 1$, we denote by $\epsilon \bar{c}(r, \theta, \phi, t)$, $\epsilon \bar{p}(r, \theta, \phi, t)$, and $\epsilon \bar{R}(\theta, \phi, t)$, the perturbations from the radially-symmetric solutions of (2.1), (2.4)–(2.10). Thus, the total nutrient concentration, internal pressure and tumour radius are given by

$$\begin{aligned} c_\epsilon &= c(r, t) + \epsilon \bar{c}(r, \theta, \phi, t), \\ p_\epsilon &= p(r, t) + \epsilon \bar{p}(r, \theta, \phi, t), \\ R_\epsilon &= R(t) + \epsilon \bar{R}(\theta, \phi, t), \end{aligned}$$

so that $r = (R(t) + \epsilon \bar{R}(\theta, \phi, t), \theta, \phi)$ on $\Gamma(r, t) = 0$. By substituting with the above expressions in (2.1), (2.4)–(2.10), we recover equations (2.11)–(2.18) at leading order. Continuing to $O(\epsilon)$, we derive the equations which govern the perturbations \bar{c} , \bar{p} , and \bar{R}

$$0 = \nabla^2 \bar{c} - \lambda'(c) \bar{c}, \quad (4.1)$$

$$0 = \mu \nabla^2 \bar{p} + S'(c) \bar{c}, \quad (4.2)$$

$$\frac{\partial \bar{R}}{\partial t} = -\mu \left(\frac{\partial \bar{p}}{\partial r} + \bar{R} \frac{\partial^2 p}{\partial r^2} \right) \Big|_{r=R(t)}, \quad (4.3)$$

subject to

$$\frac{\partial \bar{c}}{\partial r} = 0, \quad \text{at } r = 0, \quad (4.4)$$

$$\bar{c}(R, \theta, \phi, t) = \frac{\gamma c_\infty}{R^2} (2\bar{R} + \mathcal{L}(\bar{R})) - \bar{R} \left. \frac{\partial c}{\partial r} \right|_{r=R(t)}, \quad (4.5)$$

$$\frac{\partial \bar{p}}{\partial r} = 0, \quad \text{at } r = 0, \quad (4.6)$$

$$\bar{p}(R, \theta, \phi, t) = -\bar{R} \left. \frac{\partial p}{\partial r} \right|_{r=R(t)}, \quad (4.7)$$

$$\bar{R}(\theta, \phi, 0) = \bar{R}_0(\theta, \phi), \quad \text{prescribed,} \quad (4.8)$$

where primes denote differentiation with respect to c , and $\mathcal{L}(\cdot)$ denotes the angular part of the Laplacian operator

$$\mathcal{L}(f) = \frac{1}{\sin \theta} \frac{\partial}{\partial \theta} \left(\sin \theta \frac{\partial f}{\partial \theta} \right) + \frac{1}{\sin^2 \theta} \frac{\partial^2 f}{\partial \phi^2}, \quad (4.9)$$

so that

$$\nabla^2 f = \frac{1}{r^2} \frac{\partial}{\partial r} \left(r^2 \frac{\partial f}{\partial r} \right) + \frac{\mathcal{L}(f)}{r^2}.$$

Rather than eliminating \bar{p} from the model equations, in this section we perform our analysis, explicitly retaining \bar{p} . Recalling from Section 3 that $\lambda(c) = \lambda$ and $S(c) = s(c - \bar{c})$, we remark that $\lambda'(c) = 0$ and $S'(c) = s$ in (4.1) and (4.2). Thus, we seek separable solutions to (4.1)–(4.8) of the form

$$\begin{aligned} \bar{c} &= \sum \chi_{lm}(t) r^l Y_{lm}(\theta, \phi), & \bar{p} &= \sum \left\{ \Pi_{lm}(t) - \frac{s \chi_{lm} r^2}{2\mu(2l+3)} \right\} r^l Y_{lm}(\theta, \phi), \\ \bar{R} &= \sum \rho_{lm}(t) Y_{lm}(\theta, \phi), \end{aligned}$$

where the spherical harmonics $Y_{lm}(\theta, \phi)$ satisfy $\mathcal{L}(Y_{lm}) = -l(l+1)Y_{lm}$ so that

$$\nabla^2(r^l Y_{lm}) = 0,$$

and the coefficients χ_{lm} , Π_{lm} , and ρ_{lm} are determined below.

We remark that \bar{c} and \bar{p} automatically satisfy (4.1), (4.2), (4.4), and (4.6). Imposing (4.5) and (4.7) and exploiting the orthogonality of the spherical harmonics Y_{lm} to equate the coefficients of Y_{lm} to zero eventually yields the following pair of expressions which define χ_{lm} and Π_{lm} in terms of ρ_{lm} :

$$\begin{aligned} R^l \chi_{lm} &= - \left\{ \frac{\gamma c_\infty}{R^2} (l-1)(l+2) + \frac{\lambda R}{3} \right\} \rho_{lm}, \\ R^l \Pi_{lm} &= \frac{s R^{l+2} \chi_{lm}}{2\mu(2l+3)} + \frac{s}{3\mu} \left\{ c_\infty - \bar{c} - \frac{2\gamma c_\infty}{R} - \frac{\lambda R^2}{15} \right\} \rho_{lm}. \end{aligned}$$

Using these identities in (4.3) yields the following ODE for ρ_{lm} :

$$\frac{1}{s \rho_{lm}} \frac{d\rho_{lm}}{dt} = -\frac{(l-1)}{3} \left\{ c_\infty - \bar{c} - \frac{l}{2l+3} \frac{\gamma c_\infty}{R} - \frac{2l+9}{2l+3} \frac{\lambda R^2}{15} \right\}, \quad (4.10)$$

where the evolution of $R(t)$ is governed by (3.3).

From (4.10), we remark further that when $l = 1$ $\frac{d\rho_{lm}}{dt} = 0$ so that the system is always stable with respect to the first spherical harmonic $Y_{1m}(\theta, \phi)$. This is consistent with results derived

by Greenspan, Langer, and Schwegler *et al.* [27,28,34,35] who studied similar models and occurs because the mode for which $l = 1$ represents a translation of the axes.

The evolution of the coefficients ρ_{lm} is clearly independent of the azimuthal component of the modal solutions $Y_{lm}(\theta, \phi)$. Since $R(t)$ is a dynamic variable, we remark further that particular modes Y_{lm} may be excited for certain ranges of R and damped for others. This situation is depicted in Figure 4 where, for a particular set of parameter values, we sketch the right-hand side of (4.10) for several choices of l ($l = 2, 5, 10, 15, 20$). Also included in the diagram is a dashed curve showing how $\frac{dR}{dt}$ varies with R , over the feasible range defined by (3.2). This curve demonstrates the existence of a radially-symmetric solution ($R \sim 3.12$) which is stable with respect to time-dependent perturbations. The other curves, showing how $(1/\rho_{lm})\frac{d\rho_{lm}}{dt}$ varies with R , suggest that this steady state is, in fact, unstable with respect to a finite range of asymmetric perturbations ($2 \leq l \leq 14$).

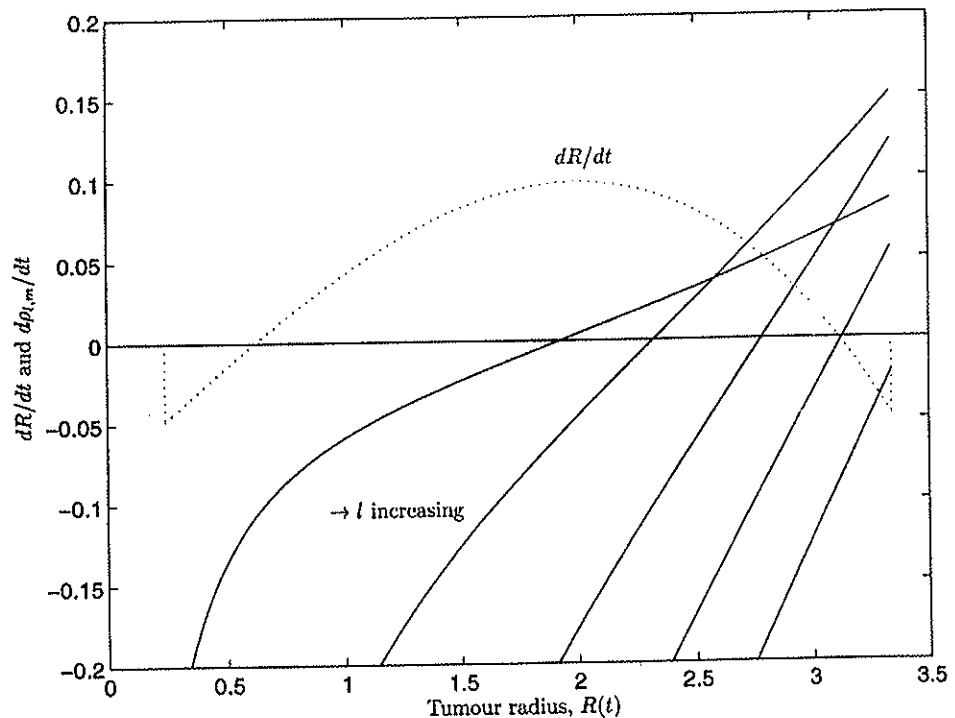


Figure 4. Diagram showing how the growth rates of the asymmetric modes $Y_{lm}(\theta, \phi)$ vary with R . For five choices of $l = (2, 5, 10, 15, 20)$, $(1/\rho_{lm})\frac{d\rho_{lm}}{dt}$ is sketched against R . The dashed curve is included to show how $\frac{dR}{dt}$ varies with R over the feasible range of tumour radii. Parameter values: $c_\infty = 1.2$, $\tilde{c} = 0.8$, $c_{nec} = 0.2$, $\lambda = 0.5$, $\gamma = 0.1$, $s = 1.0$.

The above stability analysis is reminiscent of techniques used by Murray, and other authors, to predict spatial patterning in mathematical models of biological systems. Whilst some authors [43-45] have considered how the growth rate of the domain affects the evolving pattern, they considered only simple cases for which the domain's growth rate was prescribed *a priori*. By contrast, here the growth rate of the domain is determined as part of the solution.

Equation (4.10) also demonstrates the stabilising effect that cell-cell adhesion has on the tumour's growth. When $\gamma = 0$, (4.10) reduces to give

$$\frac{1}{s\rho_{lm}} \frac{d\rho_{lm}}{dt} = -\frac{(l-1)}{3} \left\{ c_\infty - \tilde{c} - \left(\frac{2l+9}{2l'+3} \right) \frac{\lambda R^2}{15} \right\}.$$

Setting $\frac{dR}{dt} = 0$ in (3.3), we observe that the nontrivial steady state radius is given by

$$R^2 = R_\infty^2 \equiv \frac{15}{\lambda_0} (c_\infty - \tilde{c}).$$

In this case, we deduce that

$$\frac{1}{s\rho_{lm}} \frac{d\rho_{lm}}{dt} = 2(l-1)(2l+9)(c_\infty - \bar{c}) > 0, \quad \forall l > 2.$$

Thus we conclude that, *in the absence of cell-cell adhesion*, the radially-symmetric steady state solution is *unstable to all asymmetric modes* Y_{lm} for which $l > 2$. This contrasts with the results presented in Section 3 where we showed that the larger, radially-symmetric steady state was stable with respect to time-dependent perturbations.

More generally, with $\gamma > 0$, the stabilising effect of cell-cell adhesion is restored. Indeed, we deduce from (4.10) that if $\gamma > 0$ and $\frac{dR}{dt} = 0$, then

$$\frac{1}{s\rho_{lm}} \frac{d\rho_{lm}}{dt} = \frac{(l-1)}{(2l+3)} \left(\frac{2\lambda R^2}{15} - (l+2) \frac{\gamma c_\infty}{R} \right).$$

Thus, the steady state is stable with respect to all asymmetric modes for which l is sufficiently large, i.e., $l+2 > 2\lambda R^3/15\gamma c_\infty$. Further, for a particular value of R only a finite number of modes are excited, the choice of parameter values dictating the unstable range of l . This is demonstrated in Figure 4 where the modes $Y_{2,m}$, $Y_{5,m}$, and $Y_{10,m}$ are excited for the larger steady state, whereas the modes $Y_{15,m}$ and $Y_{20,m}$ are not. This figure also suggests how as R increases towards the larger steady state radius ($R \sim 3.12$), the number of modes which are excited changes. Further, depending on their growth rate, the asymmetric perturbations may become comparable in magnitude with the leading-order radially-symmetric solutions, in which case our asymptotic expansion ceases to be valid and the full model, (2.1), (2.4)–(2.10), must be used to construct valid solutions.

By differentiating (4.10) with respect to l , it is possible to determine which is the fastest growing mode for a particular choice of R

$$\frac{\partial}{\partial l} \left(\frac{1}{s\rho_{lm}} \frac{d\rho_{lm}}{dt} \right) = -\frac{1}{3}(c_\infty - \bar{c}) + \frac{(2l^2 + 6l - 3)}{3(2l+3)^2} \frac{\gamma c_\infty}{R} + \frac{(4l^2 + 12l + 39)}{3(2l+3)^2} \frac{\lambda R^2}{15}.$$

Setting $\frac{\partial}{\partial l} \left(\frac{1}{s\rho_{lm}} \frac{d\rho_{lm}}{dt} \right) = 0$, and noting that $l \neq -3/2$, we deduce that for a fixed value of R the fastest growing mode l_{fastest} satisfies a quadratic equation of the form

$$0 = (2l^2 + 6l - 3) \frac{\gamma c_\infty}{R} + (4l^2 + 12l + 39) \frac{\lambda R^2}{15} - (2l+3)^2 (c_\infty - \bar{c}). \quad (4.11)$$

Using (4.10) and (4.11), in Figure 5 we focus on the stability of the upper branch of steady solutions constructed in Figure 3 with respect to asymmetric perturbations as the parameter γ varies. Referring to (3.4) and for direct comparison with Figure 3, we use $p_0 = 30\gamma c_\infty/\lambda$ in place of γ (since all the other system parameters are fixed, p_0 is proportional to γ). For each value of p_0 (or, equivalently, γ), we plot the range of l to which the corresponding steady state is unstable. The fastest growing mode, as predicted using (4.11), is also included. From the diagram, we note that as p_0 increases, and the steady state radius decreases, the range of instability, together with the order of the fastest growing mode, become smaller, until, for p_0 sufficiently large ($p_0 > 5.0$), the steady state is actually stable with respect to all asymmetric modes Y_{lm} .

In Figure 6, we show how the size and shape of an initially radially-symmetric tumour alters when it is subjected to an asymmetric disturbance. At a given time, the mode which dominates the instability is selected from (4.11). As $R(t)$ changes, so the dominant mode also changes. Referring to [27], we remark that if the instability which develops is controlled by nonlinear processes, not included in the present model, the tumour may reach an equilibrium again. Otherwise, it may split into smaller tumours. These secondary tumours would eventually also split, thereby continuing the growth and invasion of the cancer.

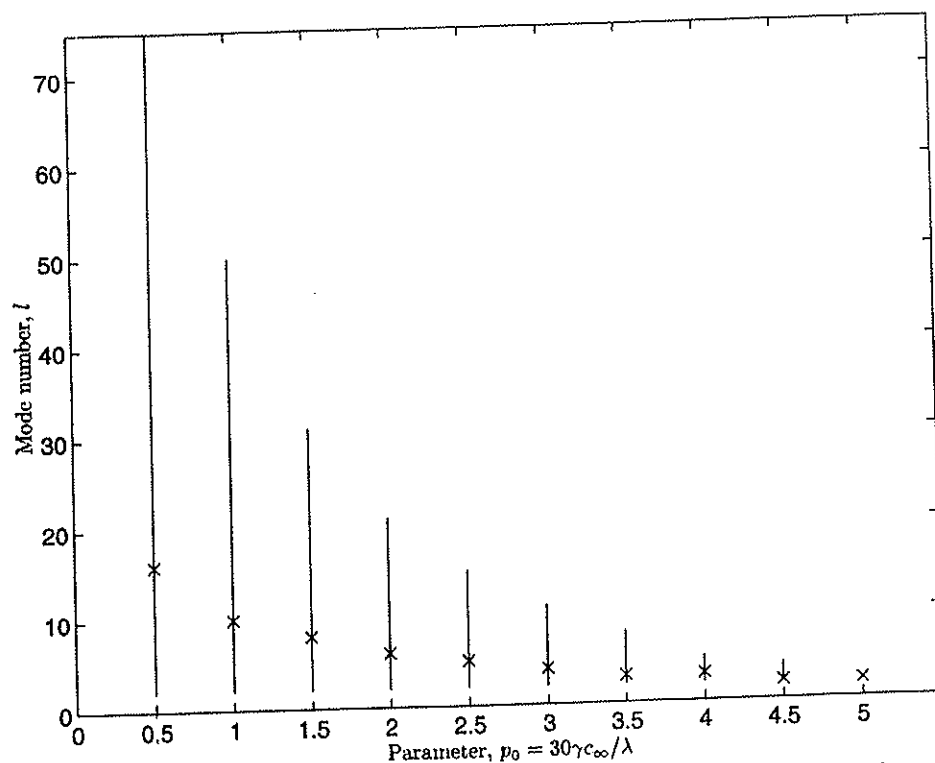


Figure 5. Diagram depicting those asymmetric modes ρ_{lm} to which the upper branch of steady solutions shown in Figure 3 are unstable. With p_1 fixed ($p_1 = 6.0$), as p_0 (or γ) increases both the magnitude of the most rapidly growing mode and also the range of the unstable modes diminishes, until for $p_0 > 5.0$ decay of all asymmetric disturbances of the steady state is predicted. Parameter values: $c_\infty = 1.0$, $\bar{c} = 0.8$, $c_{nec} = 0.2$, $\lambda = 0.5$, $s = 1.0$.

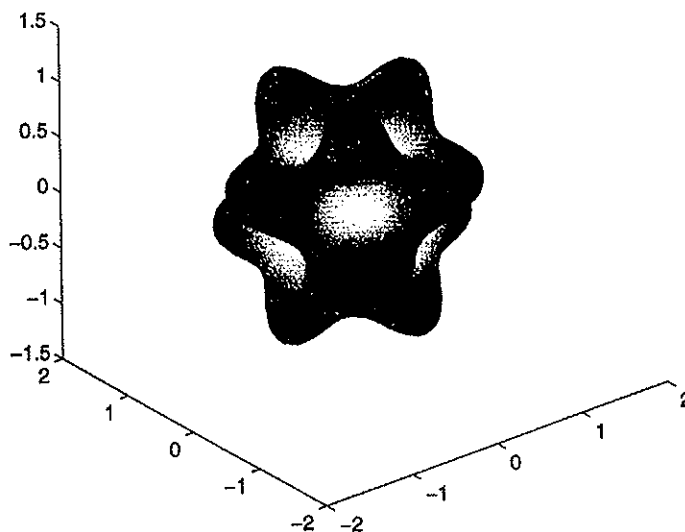


Figure 6. Schematic representation of an invading carcinoma with particular mode $Y_{6,3}$.

5. CONCLUSIONS

In this paper we have developed a mathematical model to describe the evolution of a homogeneous avascular tumour which comprises proliferating cells only, and whose growth rate is regulated by an externally-supplied nutrient. We showed how the balance between the cell-cell

adhesion forces, which act on the tumour boundary to maintain the tumour's compactness, and the internal expansive forces due to cell proliferation influences the existence and stability of steady, radially-symmetric tumour configurations. The incorporation into our model of cell-cell adhesion using the Gibbs-Thomson relation is new and is employed here to account for the energy consumed by cells on the periphery to preserve the tumour's compactness. The Gibbs-Thomson relation states that the nutrient concentration at a point on the tumour boundary is less than the assumed constant external concentration by a factor which depends on the local curvature there. We also showed how internal pressure and cell velocity could be eliminated and the standard models of nutrient-limited multicellular spheroid growth recovered as special cases of our original model. In this way we establish the validity of the existing models of multicellular spheroid growth from a more physically-based foundation.

Solution of the reduced, radially-symmetric model shows how the existence and stability, with respect to time-dependent perturbations, of steady solutions depends on the system parameters, and two parameter groupings in particular. For example, referring to Figures 2 and 3, we note that if the bonds of cell-cell adhesion are sufficiently strong, relative to the other physical effects ($\gamma^2 > 5(c_\infty - \bar{c})^3/9\lambda c_\infty^2 \equiv \gamma_{\text{crit}}^2$, say), then no steady state solutions exist and we conclude that the host environment will not support a tumour. By contrast, if the cell-cell adhesion bonds are sufficiently weak ($\gamma^2 < \gamma_{\text{crit}}^2$), then two steady solutions exist, of which the smaller tumour is unstable with respect to temporal perturbations whereas the larger tumour is not.

Further insight into the robustness of the steady solutions is gained by studying how small asymmetric perturbations from radial symmetry evolve in time. This analysis shows clearly how the cell-cell adhesion term acts to stabilise the system and how this is countered by the cell proliferation rate which acts to destabilise the system. Our analysis predicts that, in the absence of cell-cell adhesion, all asymmetric modes grow in time. By contrast, including cell-cell adhesion ensures that only a finite number of these asymmetric modes will be excited, and that the number of modes which are unstable depends upon the relative strengths of the restraining cell-cell adhesion force and the expansive cell proliferation force. Referring to Figures 3 and 5, we note that for a range of values of γ , the larger, radially-symmetric solution is stable with respect to all asymmetric perturbations under consideration.

We remark also that the asymmetric stability analysis described above is similar to techniques employed by Murray and others to predict spatial patterning in mathematical models of biological systems. Whilst Murray and others have considered how the growth rate of the domain affects the evolving pattern, they considered only simple cases for which the domain's growth rate was prescribed *a priori* [43-45]. By contrast, in this paper the growth rate of the domain is determined as part of the solution.

In summary, we conclude that knowledge of the strength of the cell-cell adhesion forces, relative to the other forces acting within a tumour, could be clinically important in estimating a tumour's ability to invade its host environment. Indeed, we believe that γ could be used as a physical index which characterises a particular cell-line's potential for growth and invasion. When assessing the potential threat to a patient of a tumour knowledge of this parameter could assist clinicians deciding whether surgery is an appropriate course of action.

REFERENCES

1. J. Folkman and M. Hochberg, Self-regulation of growth in three dimensions, *J. Exp. Med.* **138**, 745-753 (1973).
2. J.F.R. Kerr, Shrinkage necrosis; a distinct mode of cellular death, *J. Path.* **105**, 13-20 (1971).
3. J.F.R. Kerr, Wyllie and A.R. Currie, Apoptosis: A basic biological phenomenon with wide-ranging implications in tissue kinetics, *Br. J. Cancer* **26**, 239-257 (1972).
4. R.M. Sutherland, Cell and environment interactions in tumor microregions: The multicell spheroid model, *Science* **240**, 177-184 (1988).
5. J. Folkman, Tumour angiogenesis, *Adv. Cancer Res.* **19**, 331-358 (1974).

6. J. Folkman, The vascularisation of tumours, In *Cancer Biology*, (Edited by E.C. Friedberg), pp. 115-124, Scientific American, (1976).
7. V.R. Muthukarruppan, L. Kubai and R. Auerbach, Tumour-induced neovascularisation in the mouse eye, *J. Natl. Cancer Inst.* **69**, 699-705 (1982).
8. M. Tubiana, The kinetics of tumour cell proliferation and radiotherapy, *Br. J. Radiol.* **44**, 325-347 (1971).
9. R.K. Jain, Physiological resistance to the treatment of solid tumours, In *Drug Resistance in Oncology*, (Edited by B.A. Teicher), Marcel Dekker, (1993).
10. R.K. Jain, Barriers to drug delivery in solid tumours, *Scientific American* **271** (1), 58-65 (1994).
11. J.A. Adam, A mathematical model of tumour growth II. Effects of geometry and spatial uniformity on stability, *Math. Biosci.* **86**, 183-211 (1987).
12. J.A. Adam, A mathematical model of tumor growth III: Comparison with experiment, *Math. Biosci.* **86**, 213-227 (1987).
13. J.A. Adam and S.A. Maggelakis, Diffusion regulated growth characteristics of a spherical prevascular carcinoma, *Bull. M. Bio.* **52**, 549-582 (1990).
14. H.M. Byrne and M.A.J. Chaplain, Growth of non-necrotic tumours in the presence and absence of inhibitors, *Math. Biosci.* **130**, 151-181 (1995).
15. H.M. Byrne and M.A.J. Chaplain, Growth of necrotic tumours in the presence and absence of inhibitors, *Math. Biosci.* (submitted).
16. M.A.J. Chaplain and N.F. Britton, On the concentration profile of a growth inhibitory factor in multicell spheroids, *Math. Biosci.* **115**, 233-245 (1993).
17. H.P. Greenspan, Models for the growth of a solid tumour by diffusion, *Stud. Appl. Math.* **52**, 317-340 (1972).
18. S.A. Maggelakis and J.A. Adam, Mathematical model of prevascular growth of a spherical carcinoma, *Mathl. Comput. Modelling* **13** (5), 23-38 (1990).
19. J.J. Casciari, S.V. Sotirchos and R.M. Sutherland, Mathematical modelling of microenvironment and growth in EMT6/Ro multicellular tumour spheroids, *Cell Prolif.* **25**, 1-22 (1992).
20. M. Murusic, Z. Bajzer, J.P. Freyer and S. Vuk-Pavlovic, Analysis of growth of multicellular tumour spheroids by mathematical models, *Cell Prolif.* **27**, 73-94 (1994).
21. D. Balding and D.L.S. McElwain, A mathematical model of tumour-induced capillary growth, *J. Theor. Biol.* **114**, 53-73 (1985).
22. H.M. Byrne and M.A.J. Chaplain, Mathematical models for tumour angiogenesis: Numerical simulations and nonlinear wave solutions, *Bull. Math. Biol.* **57**, 461-486 (1995).
23. M.A.J. Chaplain and A.M. Stuart, A model mechanism for the chemotactic response of endothelial cells to tumour angiogenesis factor, *IMA J. Math. Appl. Med. Biol.* **10**, 149-168 (1993).
24. M.A.J. Chaplain, Avascular growth, angiogenesis and vascular growth in solid tumours: The mathematical modelling of the stages of tumour development, *Mathl. Comput. Modelling* **23** (6), 47-88 (1996).
25. C.L. Stokes and D.A. Lauffenburger, Analysis of the roles of microvessel endothelial cell random motility and chemotaxis in angiogenesis, *J. Theor. Biol.* **152**, 377-403 (1991).
26. R. Muir, *Muir's Textbook of Pathology*, 13th edition, (Edited by R.N.M. MacSween and K. Whaley), Edward Arnold, London, (1992).
27. H.P. Greenspan, On the growth and stability of cell cultures and solid tumours, *J. Theor. Biol.* **56**, 229-242 (1976).
28. J.S. Langer, Instabilities and pattern formation in crystal growth, *Rev. Mod. Phys.* **52**, 1-20 (1980).
29. W.W. Mullins and R.F. Sekerka, Morphological stability of a particle growing by diffusion or heat flow, *J. Appl. Phys.* **34**, 323-329 (1963).
30. J.A. Glazier and F. Graner, Simulation of the differential adhesion driven rearrangement of biological cells, *Phys. Rev. E* **47**, 2128-2154 (1993).
31. F. Graner and J.A. Glazier, Simulation of biological cell sorting using a 2-dimensional extended Potts-model, *Phys. Rev. Lett.* **69**, 2013-2016 (1992).
32. J.C.M. Mombach, J.A. Glazier, R.C. Raphael and M. Zajac, Quantitative comparison between differential adhesion models and cell sorting in the presence and absence of fluctuations, *Phys. Rev. Lett.* **75**, 2244-2247 (1995).
33. T. Sekimura and H. Hotani, The morphogenesis of liposomes viewed from the aspect of bending energy, *J. Theor. Biol.* **149**, 325-337 (1991).
34. H. Schweler, K. Tarumi and B. Gersmann, Physico-chemical model of a protocell, *J. Math. Biol.* **22**, 335-348 (1985).
35. H. Schwegler and K. Tarumi, The "protocell": A mathematical model of self-maintenance, *BioSystems* **19**, 307-315 (1986).
36. M. Miyasaka, Cancer metastasis and adhesion molecules, *Clin. Orth. Rel. Res.* **312**, 10-18 (1995).
37. R.B. Nagle, J.D. Knox, C. Wolf, G.T. Bowden and A.E. Cress, Adhesion molecules, extracellular matrix and proteases in prostate carcinoma, *J. Cell. Biochem.* **19S**, 232-237 (1994).
38. R.M. Sutherland and R.E. Durand, Growth and cellular characteristics of multicell spheroids, *Recent Results in Cancer Research* **95**, 24-49 (1984).
39. D.L.S. McElwain and L.E. Morris, Apoptosis as a volume loss mechanism in mathematical models of solid tumour growth, *Math. Biosci.* **39**, 147-157 (1978).
40. S.P. Neumann, Theoretical derivation of Darcy's Law, *Acta Mechan.* **25**, 153-170 (1977).

- 115-124,
mouse eye,
347 (1971).
Oncology,
)
iformity on
Biosci. 86,
cular carci-
f inhibitors,
f inhibitors,
in multicell
-340 (1972).
oma, *Mathl.*
and growth
ur spheroids
1, *J. Theor.*
simulations
elial cells to
athematical
3).
lom motility
ey), Edward
56, 229-242
1980).
or heat flow,
ological cells,
Potts-model,
n differential
5, 2244-2247
iding energy,
. 22, 335-348
oSystems 19,
995).
ellular matrix
Recent Results
odels of solid
41. C.M. Elliott and J.R. Ockendon, Weak and variational methods for moving boundary value problems, *Research Notes in Mathematics*, Volume 59, Pitman, London, (1982).
 42. K. Groebe and W. Mueller-Klieser, Distributions of oxygen, nutrient and metabolic waste concentrations in multicellular spheroids and their dependence on spheroid parameters, *Eur. Biophys. J.* 19, 169-181 (1991).
 43. P. Arcuri and J.D. Murray, Pattern sensitivity to boundary and initial conditions in reaction-diffusion models, *J. Math. Biol.* 24, 141-165 (1986).
 44. M.A.J. Chaplain, The development of a spatial pattern in a model for cancer growth, In *Experimental and Theoretical Advances in Biological Pattern Formation*, (Edited by H.G. Othmer, P.K. Maini and J.D. Murray), pp. 45-60, Plenum Press, (1993).
 45. J.D. Murray, *Mathematical Biology*, Springer-Verlag, Berlin, Germany, (1990).
 46. D.L.S. McElwain and G.J. Pettet, Cell migration in multicell spheroids—Swimming against the tide, *Bull. Math. Biol.* 55, 655-674 (1993).